On the Determination of the Average Molecular Weight, Radius of Gyration, and Mass/Length Ratio of Polydisperse Solutions of Polymerizing Rod-like Macromolecular Monomers by Multi-Angle Static Light Scattering

Fabio Ferri[1], Maria Greco[1], Mattia Rocco[2]*

[1]Dipartimento di Scienze Chimiche, Fisiche e Matematiche and INFM, Università dell'Insubria, sede di Como, Via Lucini 3, I-22100 Como, Italy; [2]Gruppo di Biostrutture, Istituto Nazionale per la Ricerca sul Cancro (IST), Centro per le Biotecnologie Avanzate (CBA), Largo Rosanna Benzi 10, I-16132 Genova, Italy.

SUMMARY: The angular dependence of the light scattered from polydisperse solutions of rod-like or worm-like linear polymers formed by the polymerization of rod-like macromolecular monomers was studied with the aid of computer simulations. Except at very low conversion degrees, these ensembles are characterized by curved Zimm-like plots. An appraisal of the use of polynomial fittings for the derivation of the weight-average molecular weight (M_w) and of the z-average square radius of gyration ($\langle R_g^2 \rangle_z$) from such plots is presented and discussed. Depending on the average size and shape distribution, the use of polynomial fittings allows the applicability of the Zimm method well beyond the standard condition $q^2\langle R_g^2 \rangle_z << 1$, q being the scattering wavevector. In addition, the derivation of the w/z-average mass/length ratio M_L of the polymers from only partially linear Casassa plots, from which large errors in the derived M_L values can be made, is analyzed. By combining the Casassa method with the complementary Holtzer plots, it is usually possible to assess the reliability of the results and give an estimate of their accuracy. However, it was also found that apparently linear Casassa plots, allowing a good estimate of the M_L value, may arise in particular situations even when the Holtzer plot would indicate otherwise.

Introduction

The present investigation was spurred by the need of finding suitable procedures for the analysis of static light scattering data when sample polydispersity severely complicates their interpretation. In particular, with the advent of commercially available multi-angle light scattering photometers, the time-resolved determination of size- and shape-dependent quantities, such as the weight-average molecular weight M_w, the z-average square radius of gyration $\langle R_g^2 \rangle_z$ and the w/z-average mass/unit length M_L, is within reach. However, for many

 CCC 1022-1360/00/$ 17.50+.50/0

inherently polydisperse systems, which include, for example, polymerization reactions and the nucleation and growth of crystals, the extrapolation of the sought parameters from classical procedures can be quite difficult if not outright dangerous.

We will be dealing in this paper with a particular system in which a rod-like bifunctional macromolecular monomer polymerizes linearly, giving rise to single-stranded rod-like or worm-like polymers. By varying the relative activation rate of the two binding sites of the monomer, different size distributions can be obtained, from the classical Flory most probable distribution[1)] to highly skewed ones[2)]. This or similar situations are often found in biological systems, and in particular it was an investigation of the fibrinogen-fibrin conversion that brought this problem to our attention[3)]. In this system, a high molecular weight (~340,000), rod-like macromolecular monomer ~50 nm long polymerizes following enzymatic activation[4-5)]. In the initial stages, linear polymers form, which later aggregate side-by-side and branch, giving rise to a three-dimensional network. Depending on the solution conditions and on the type and activity of the enzyme, the elongation stage can last from seconds to minutes, but even in this stage the Zimm-like plots rapidly deviate from linearity[3,6)], rendering difficult an estimate of M_w and $\langle R_g^2 \rangle_z$. Startlingly, the corresponding Casassa plots quickly attain an high degree of linearity, but the derived M_L values are initially very high and then decay to lower values, a behavior clearly inconsistent with any reasonable linear polymerization mechanism[3)]. Computer simulations were employed to assess the validity of polynomial fittings in the Zimm plot case, and to understand the behavior of the Casassa plot. Although in our simulations we tried to match as close as possible the experimental conditions outlined above, our results have a more general relevance for the interpretation of static light scattering data from polydisperse systems.

Methods

A – Light scattering theory.

According to the theory of static light scattering, the time-average intensity scattered by a solution of macromolecules (or particles) is customarily expressed as a function of the wavevector $q = 4\pi n/\lambda \sin(\theta/2)$, where θ is the scattering angle between the incident and the scattered directions, λ is light wavelength *in vacuo* and n is the medium refraction index (see[7)]). When the solution is so dilute that interactions between particles can be neglected, the scattered intensity is given by the sum of the intensities scattered by the single particles:

$$R(q) = K\, c\, M_w < P(q) >_z \tag{1}$$

where R(q) is called Rayleigh ratio and represents the intensity scattered in absolute units (cm^{-1}). In Eq. 1 c is the sample concentration (g cm^{-3}), K is the optical constant (cm^2 mol g^{-2}) given by $K = 4\pi^2 n^2 (dn/dc)^2/(N_A \lambda^4)$, N_A being the Avogadro number and dn/dc the refractive index increment of the solute, while M_w is the weight-average molecular weight, and $<P(q)>_z$ the z-average of the particle form factor. The latter two are defined as:

$$M_w = \sum_i w_i\, M_i \tag{2}$$

$$< P(q) >_z = \frac{\sum_i w_i\, M_i\, P_i(q)}{\sum_i w_i\, M_i} \tag{3}$$

w_i being the weight fraction of particle i with molecular weight M_i. The form factor $P_i(q)$ describes the angular distribution of the light scattered by the particle i and is normalized to unity for $q = 0$. $P_i(q)$ depends on particle geometry and, for particles of known shape and size, can be worked out via the Rayleigh-Gans-Debye (RGD) approximation (see[7]). However, in the limit of low q, the angular distribution of the scattered intensity becomes independent of particle shape, and, it is possible to use the well known Zimm relation[8]:

$$\frac{Kc}{R(q)} = \frac{1}{M_w}\left[1 + \frac{1}{3} q^2 < R_g^2 >_z\right] \tag{4}$$

from which the weight-average molecular weight M_w and the z-average square radius of gyration $<R_g^2>_z$ can be determined via a linear fit of the $Kc/R(q)$ vs. q^2 plot (Zimm plot). Eq. 4 is valid only over a limited range of particle dimensions and/or wavevectors q, i.e. when the second term inside the right-hand side parentheses is $<<1$. When this term approaches unity, the Zimm plot deviates from a linear behavior and its curvature depends on the particular geometry of the particles being studied. This is shown in Fig. 1 where normalized Zimm plots of monodisperse particles with different structures are plotted as a function of the reduced wavevector $u = [qR_g]^2$. As expected, all the curves converge to the theoretical behavior (straight solid line) for $u << 1$, but start to deviate from it when $u \sim 1$. The extent and the behavior of these deviations depend on the particle structure, as evidenced in the inset of the figure. For spheres (dashed curve) the deviations are the worst, while for rods

(dashed-dotted curve) are the smaller, being confined within ~ 5% even at u ~6, or above it. Thus, on the basis of Fig. 1, we can state that the use of a simple linear fitting clearly limits the accuracy, and therefore the applicability of the Zimm method, only to the range $u \leq 1$. However, under many circumstances, this range is not, or is only partially accessible, and a good amount of information coming from the region $u > 1$ would be lost. This is one of the key issues of this paper, and we will see in the next section that the use of a polynomial fitting extends the applicability of the Zimm treatment, for the cases of linear chains where the deviations are "well behaved", well beyond the ideal condition $u \leq 1$.

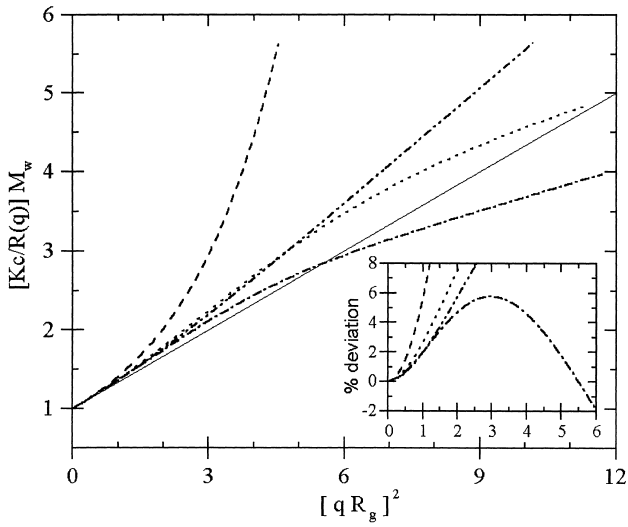

Fig. 1: Master Zimm plots for monodisperse particles of different structures: spheres (dashed lines), random coils (dot-dot-dash), wormlike chains with the ratio l_p/L_c = 1/3 (dots), and rigid rods (dot-dash). In the inset, the % deviations with respect the theoretical behavior indicated by the straight solid line are reported for the low $[qR_g]^2$ region.

In addition to the Zimm method, a second method first derived by Casassa[9] can be used. The Casassa method applies to linear particles (such as rod-like or worm-like chains) and allows the determination of the ratio M/L_c, M and L_c being the molecular weight and contour length of the chain, respectively. The method applies over a range of q's and particle sizes which are opposite to that of the Zimm plot, i.e., when the second term inside the right-hand side parentheses in Eq. 4 is >> 1. However this condition alone is not sufficient, and the actual applicability of the Casassa method depends on how both the contour length and the persistence length l_p of the chain compare with the wavevector of observation. For worm-like

particles this implies that both qL_c and ql_p must be much larger that unity, so that at these wavevectors the chain behaves as a rigid rod irrespectively of its flexiblity (see below). Under these conditions, $R(q)^{-1}$ is linearly related to q, and from the slope of the plot $Kc/R(q)$ vs. q known as Casassa plot[9]:

$$\frac{Kc}{R(q)} = \frac{2}{\pi^2}\frac{1}{M_w}\frac{< L_c^{-2} >_z}{< L_c^{-1} >_z^2} + \frac{1}{\pi\, M_w < L_c^{-1} >_z} q \tag{5}$$

one can recover the average mass for unit length $M_L = M_w < L_c^{-1} >_z = \sum_i w_i\, M_i/L_{c_i}$ of the chain. The intercept of the Casassa plot is a not-straightforward function of the particles length and molecular weight, but one can notice that when all the chains have the same M_L, this reduces to $2/\pi^2 M_n$, allowing the determination of the particle number-average molecular weight M_n.

In this article we will be dealing with rigid rod-like or semiflexible worm-like chains, the first being a limiting case of the latter. The form factor of a worm-like chain characterized by a contour length L_c and a persistence length l_p can be written as[10]:

$$P(q) = \frac{2}{L_c^2}\int_0^{L_c} (L_c - t)\varphi(t, l_k, q)dt \tag{6}$$

where $l_k = 2l_p$ is the Kuhn statistical segment and the function φ is defined in reference[10]. The ratio $\beta = l_p/L_c$ defines the stiffness or semiflexibility of the chain. Depending on β and on the q of observation, the form factor $P(q)$ exhibits quite different behaviors. For $\beta >> 1$, the chain behaves as a rigid rod and, correspondingly, the large q asymptotic behavior of the form factor is $P(q) = \pi/qL_c$, the crossover falling at $qL_c \sim \pi$. For $\beta << 1$, the chain can be assimilated to a random coil characterized by monomers of length $l_k = 2l_p$. In this case, the asymptotic behavior of $P(q)$ depends on the value of $1/l_p$ compared with q, and it can be easily shown that[10]:

$$P(q) = \frac{6}{L_c l_p} q^{-2} \qquad R_g^{-1} \le q \le l_p^{-1} \tag{7.a}$$

$$P(q) = \frac{\pi}{L_c} q^{-1} \qquad q \le l_p^{-1} \tag{7.b}$$

where $R_g = (L_c l_p / 3)^{1/2}$ is the radius of gyration of the random coil chain. Eqs. 7.a and 7.b predict that, for intermediate wavevectors (case 7.a), P(q) is equal to the asymptotic form factor of random coils, while, for larger q's (case 7.b), it is equal to that expected for rigid rods. The wavevector q^* at which the crossover between the two regimes takes place is:

$$q^* l_p = \frac{6}{\pi} \sim 1.91 \tag{8}$$

showing that the rodlike behavior, and therefore the applicability of the Casassa method, is possible only when $q l_p \geq 2$ or $q l_k \geq 4$.

Combining the results obtained for the two limiting cases of $\beta >> 1$ or $\beta << 1$, we can conclude that the wavevector range in which the Casassa method works properly is set by the contour length L_c when $\beta >> 1$ (rigid rods) and by the persistence length l_p when $\beta << 1$ (random coils). In the attempt to find a length scale which rules the applicability of the Casassa method independently of β, we have defined an equivalent length l_{eqv} as:

$$\frac{1}{l_{eqv}} = \frac{2}{l_p} + \frac{4}{L_c} \tag{9}$$

Clearly l_{eqv} reduces to $l_p / 2$ when $\beta << 1$ (random coil) and to $L_c / 4$ when $\beta >> 1$ (rigid rod). The numerical factors appearing in Eq. (9) have been chosen heuristically, based on the result of Eq. (8) and on the fact that the segment (or Kuhn) length of the monomers in a random coil is twice its persistence length. Eq. (9) allows the rescaling of different Casassa plots on a single "master" curve as shown in Fig. 2A, in which $[Kc/R(q)]\, M_L\, l_{eqv}$ is plotted as a function of the reduced wavevector $q l_{eqv}$ on a log-log plot for some values of β ranging from 0.05 to ∞. It is immediately seen that the curves collapse on the same asymptote as soon as $q l_{eqv} \geq 1$. The line reported in the figure indicates a slope of 1, showing that the asymptotic behavior of the curves is correct. In order to emphasize the deviations between the theoretical and the actual behavior of the different curves, it is convenient to plot the data according to a slightly different version of the so-called Holtzer plot[11], in which $qR(q)\,(\pi Kc)^{-1}$ values are plotted against q^2. This is shown in Fig. 2B in which $qR(q)\,(Kc)^{-1}\,(\pi\, M_L)^{-1}$ is plotted against $q l_{eqv}$ (to permit direct comparison) for the same curves of panel A. The horizontal asymptote of 1 clearly indicates the theoretical behavior, and shows that all the curves are within ~ 10% of this value as soon as $q l_{eqv} \geq 1$, with deviations which depend on the particular curve being considered.

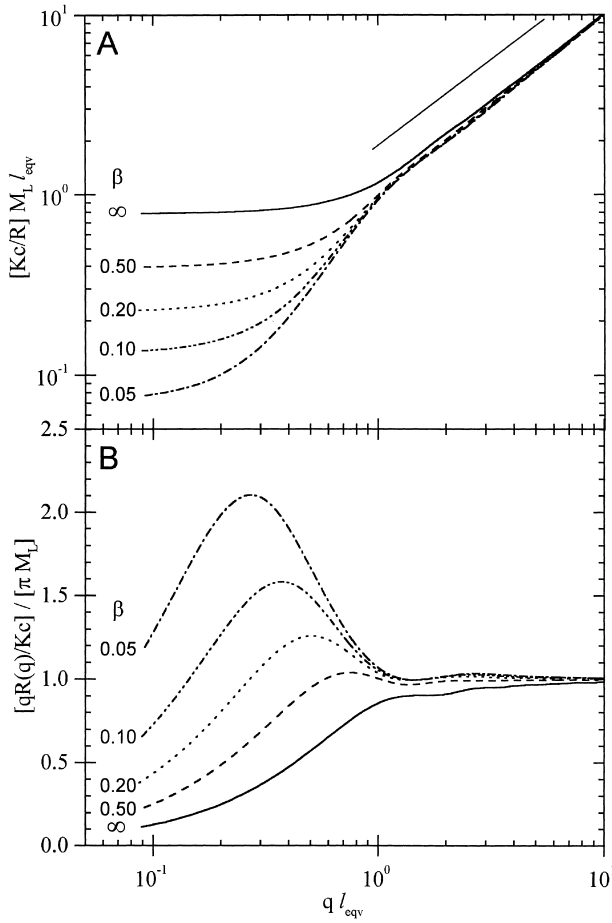

Fig. 2: Master Casassa (A) and Holtzer (B) plots for monodisperse worm-like chains of different stiffness, as indicated by the ratios $\beta = l_p / L_c$. The value of the reduced wavevector $ql_{eqv} = 1$ defines the crossover to the wavevector region in which the Casassa methods can be applied.

B – Polycondensation models and distributions.

Two different polycondensation models were considered, in which polymers grow from rod monomers of length $L_0 = 50$ nm, diameter $d_0 \sim 3$ nm, and molecular weight $M_0 = 3.0 \times 10^5$ g mol^{-1}, with $M_L = 6{,}000$ g mol^{-1} nm^{-1}. In the first model, the monomers aggregate linearly and form rod-like, end-to-end, single-stranded (RLSS) polymers of length $L_c(i) = i\,L_0$, and molecular weight $M_i = i\,M_0$, i indicating the ith polymer. For these polymers, the form factor is given by Eq. (6) with $\beta = \infty$ and the radius of gyration is $R_g^2(i) = L^2_c(i)/12$. The second

model is identical to the first one, but the polymers are allowed to be semi-flexible with a persistence length $l_p = 200$ nm equal for all of them. The form factor is still given by Eq. (6) with $\beta_i = l_p/L_c(i)$, and the radius of gyration is given by the Benoit-Doty formula[12]. We will refer to this model as the one generating worm-like, single stranded (WLSS) polymers.

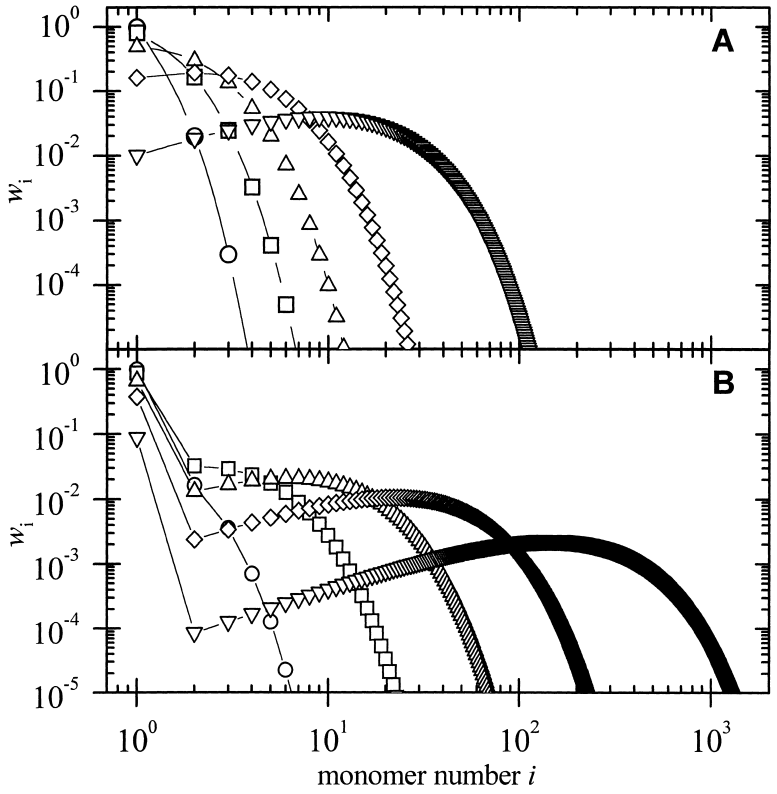

Fig. 3 Comparison between the Flory distribution (A) and the distribution predicted by Janmey with $Q = 16$ (B) at the same conversion degrees p. The Janmey distribution is much richer of monomers and is much more skewed toward high molecular weight polymers. Circles, $p = 0.01$; squares, $p = 0.1$; up triangles, $p = 0.3$; diamonds, $p = 0.6$; and down triangles, $p = 0.9$.

For each of the above models, two different size distributions were considered. The first one was the classical bifunctional Flory distribution[1] in which the two binding sites of the monomer have equal reaction probability, and become activated at random. The distribution is expressed in terms of the weight fraction $w_i(p)$ of the i^{th} polymer (made of i monomers) at each value of the monomers' conversion degree p ($0 \le p \le 1$). The second adopted distribution

was the one developed by Janmey[2], which allows for a different ratio of activation of the two monomer reaction sites, parameterized by a factor Q. This leads to a monomer concentration much higher that the one predicted by the Flory distribution (at the same p), with distributions correspondingly skewed toward much higher molecular weights. This is clearly shown in Fig. 3 where the Flory distribution and the Janmey distribution obtained for $Q = 16$ are compared for different conversion degrees ranging from p = 0.010 to 0.900.

C – Simulations.

The validity of the data analysis based of the Zimm and Casassa plots was ascertained by means of several numerical simulations, in which we tried to match as much as possible the experimental conditions. The latter ones depend on the particular polymerization process being investigated (see section B) and on the setup used for the light scattering measurements. These measurements (not reported in this work, see reference[3]) were carried out using a commercial multi-angle photometer DAWN-DSP-F (Wyatt Technology Corp., Santa Barbara, CA, USA) working at λ=632.8 nm and equipped with 17 fixed position photodiodes which can detect simultaneously the scattered light. The true scattering angles seen by the detectors depend on the refractive index of the solvent, and for the aqueous buffer solution used by us ($n_S = 1.334$ at 632.8 nm) they range from 4.7° to 158.1°. However, the two lower angles positioned at 4.7° and 14.8°, are very noisy when aqueous solvents are used, and the practical range of the instrument is thus limited to fifteen angles from 21.9° to 158.1°. The corresponding practical range of wavevectors was from $q = 5.0 \times 10^4$ to 2.6×10^5 cm^{-1}.

The synthetic data were generated according to the two models and the two distributions discussed in section B, and some discrete values of the conversion degree p between 0.01 and 0.6 were chosen. The sample concentration was assumed to be 0.36 mg/ml. Then both statistical and systematic noise was added to the data. As described in reference[3], the statistical noise is typically ~1% r.m.s. of the intensity scattered by the buffer, which, in turn, is ~10-fold lower than the intensity scattered by the fibrinogen monomers (at the above reported concentration) before polymerization is induced. Superimposed to the statistical noise, a little amount of systematic noise was also added to the data for all the angles. Its level was chosen to be ± 0.05% of signal level, with alternating positive and negative values (the detectors are alternatively positioned on the left and on the right of the beam). To have good reasonable statistics, each simulation was processed several times, by averaging over 10 different samples of statistical noise.

Results

A-Zimm-like plots

In Fig. 4 are shown some representative, Zimm-like plots for synthetic, noise-free light scattering data that we have generated according to the two polycondensation models, RLSS (squares) and WLSS (l_p = 200 nm, circles), described in Methods (section B). The weight fraction of each polymer species was calculated at different conversion degrees p (indicated in each panel) according to either the classical Flory size distribution (panels A-D) or the theory of Janmey and using a ratio Q = 16 (panels E-H and inset I). Since this latter produces distributions which are broader and skewed toward the higher molecular weights polymers (see Fig. 3), different conversion degrees were selected in order to have the same M_w as for the corresponding Flory distributions shown on the left side panels. In each panel are also shown some of the various polynomial fittings of the data that we have studied. To begin with, it is evident that the polymer mixtures produced by the Flory distributions (panels A-D) appear to be relatively well behaved, nicely fitted by 3rd degree polynomials at least up to p = 0.600 (panel D), to which correspond a $M_w = 1.2 \times 10^6$ g mol^{-1} (for these noise-free data, the 1st and 3rd degree polynomial performance at the lowest two p values is indistinguishable). For the Janmey distributions with Q = 16, the situation is quite different, with curved plots arising already at p = 0.061. Moreover, only for the worm-like polymers the 3rd degree polynomials fitted the data reasonably well across the whole range of p values investigated. For the rod-like polymers, the 3rd degree polynomial performance quickly degraded, and a 5th degree polynomial was already needed at p = 0.138 (panel G), but even that was insufficient at the higher p examined (p = 0.262, panel H). A better appraisal of this phenomenon can be gathered by looking at the inset I, where it can be seen how the addition of two lower scattering angles (filled symbols, positioned at 4.7° and 14.8°, respectively) restores the proper curvature to a 5th degree polynomial (squares; dashed line, without the additional angles; dotted line, with the additional angles). Still in inset I, it is shown that the addition of the two lower scattering angles has a comparable smaller effect for the worm-like polymers (circles; solid and dashed lines, 3rd and 5th degree polynomials, both without the additional angles). It is interesting to locate the data of Fig. 4 on the Zimm master curve of Fig. 1. This is shown by the arrows that indicate for each model (upwards for WLSS, downwards for RLSS) the wavevector at which the condition $q^2\langle R_g^2\rangle_z = 1$ is attained. Thus, it is evident why the data generated with the Janmey distribution are the more difficult to be fitted and, in particular, why the data of panel H are so poorly fitted without the addition of the first two angles.

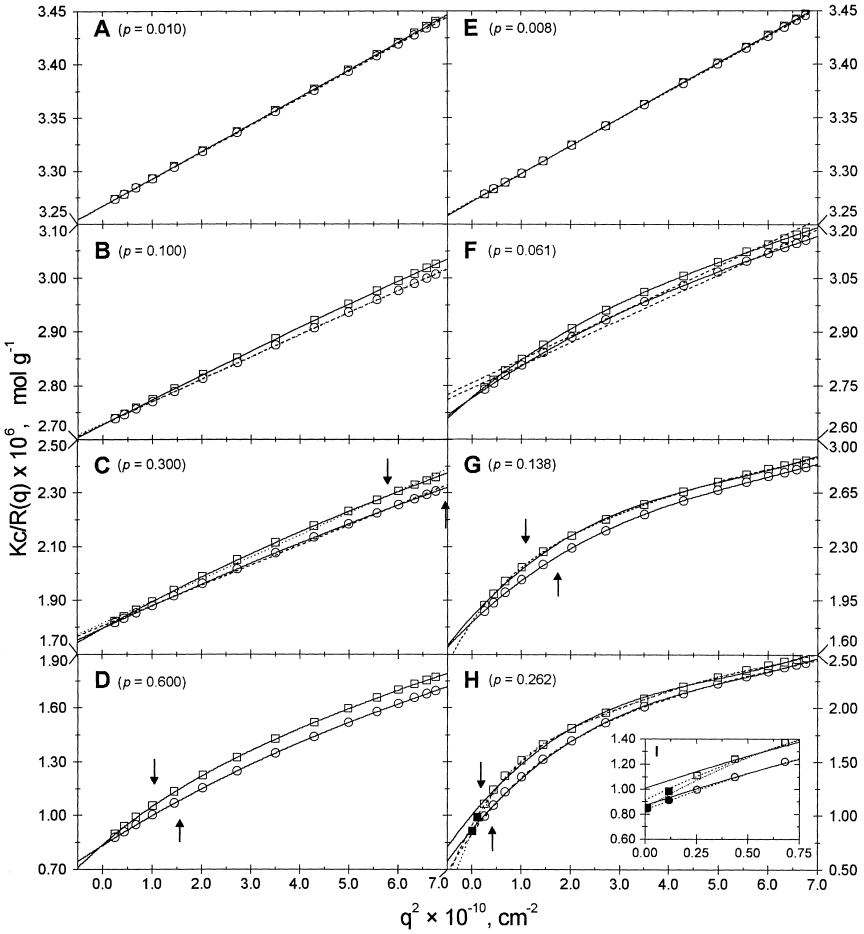

Fig. 4: Zimm-like plots for synthetic data (with no noise added) of polydisperse rod-like (RLSS, squares) and worm-like (WLSS, l_p = 200 nm, circles) polymers. The monomers are 50 nm long, 300,000 mol. wt. rods. Panels A-D, Flory distributions, panels E-I Janmey distributions with Q = 16 (the conversion degree p is indicated in each panel). In panels A, B and E, the solid and dashed lines represent 3rd degree polynomial fittings of the rod-like and of the worm-like data, respectively. In panels C and F, the solid lines are 3rd degree and the dotted and dashed lines are 1st degree polynomial fittings. In panel D, only 3rd degree polynomials are shown. In panels G and H, the solid lines are 3rd degree and the dashed lines are 5th degree polynomial fittings. In addition, in panel H and its inset I two more scattering angles are shown (solid symbols), which are however included in an additional 5th degree polynomial fitting only for the rod-like polymers (dotted line). Inset I is a close-up on the first data points of panel H. The arrows (downward for RLSS, upwards for WLSS) indicate the wavevector at which the condition $q^2\langle R_g^2\rangle_z = 1$ is attained, and their absence means that all the points obey to this condition.

A more comprehensive analysis of these plots is presented in Tables 1 and 2, where the polynomial fittings to various sets of data generated with the inclusion of both statistical and systematic noise (see Methods, section C) are presented. Table 1 deals with the polymer distributions generated according to the Flory theory, while the corresponding Janmey $Q = 16$ distributions are found in Table 2. M_w and $\langle R_g^2 \rangle_z$ were recovered as the reciprocal of the intercept, and from the ratio between the initial slope (first coefficient) and the intercept of the polynomial fit, respectively, according to Eq. 4.

Table 1. Ratios between recovered and expected parameters for different kinds of fits in the $Kc/R\theta$ versus q^2 plots for simulated data of polydisperse rod-like and worm-like polymers generated according to the Flory theory, with statistical and systematic (0.05% with alternating ± signs) noise added.

		Rod-like single stranded (RLSS) polymers			
		Conversion degree p (% total rms noise added)			
Polynomial Fitting	Parameter	0.010 (0.81)	0.100 (0.78)	0.300 (0.45)	0.600 (0.25)
1st degree	M_w	1.00 ± 0.00	1.00 ± 0.00	0.99 ± 0.00	0.91 ± 0.00
	$\langle R_g^2 \rangle_z$	1.00 ± 0.02	0.96 ± 0.01	0.89 ± 0.00	0.68 ± 0.00
	(χ^2)	(0.94 ± 0.31)	(1.11 ± 0.37)	(12.10 ± 2.47)	(1,030 ± 16.0)
3rd degree	M_w	1.00 ± 0.00	1.00 ± 0.00	1.00 ± 0.00	0.99 ± 0.00
	$\langle R_g^2 \rangle_z$	1.09 ± 0.22	1.00 ± 0.12	1.01 ± 0.02	0.92 ± 0.00
	(χ^2)	(0.89 ± 0.39)	(0.90 ± 0.41)	(1.29 ± 0.41)	(6.90 ± 1.04)
		Worm-like single stranded (WLSS) polymers (l_p = 200 nm)			
		Conversion degree p (% total rms noise added)			
Polynomial Fitting	Parameter	0.010 (0.95)	0.100 (0.81)	0.300 (0.38)	0.600 (0.20)
1st degree	M_w	1.00 ± 0.00	1.00 ± 0.00	0.99 ± 0.00	0.95 ± 0.00
	$\langle R_g^2 \rangle_z$	1.01 ± 0.01	0.98 ± 0.01	0.93 ± 0.00	0.83 ± 0.00
	(χ^2)	(1.13 ± 0.38)	(1.13 ± 0.42)	(5.20 ± 1.26)	(502 ± 11.8)
3rd degree	M_w	1.00 ± 0.00	1.00 ± 0.00	1.00 ± 0.00	1.00 ± 0.00
	$\langle R_g^2 \rangle_z$	1.02 ± 0.29	1.02 ± 0.11	1.00 ± 0.02	0.99 ± 0.00
	(χ^2)	(1.05 ± 0.48)	(1.09 ± 0.38)	(1.31 ± 0.46)	(1.86 ± 0.63)

By looking at Table 1, it is immediately evident that the M_w is well recovered even by the 1st degree polynomial fitting for all the cases examined with the exception of the rod-like polymers at the highest p studied ($p = 0.600$), for which a 9% underestimation was found. However, for the $<R_g^2>_z$ the situation is quite different, as expected from the previous analysis of Fig. 4. A striking difference between the rod-like and the worm-like polymers is immediately evident, the $<R_g^2>_z$ of the latter species being very well recovered in all cases examined by a 3rd degree polynomial. For the former species, an 8% underestimation occurs at p = 0.600 employing a 3rd degree polynomial, while a 4th degree can do no better than –4% (data not shown).

Table 2. Ratios between recovered and expected parameters for different kinds of fittings in the $Kc/R\theta$ versus q^2 plots for simulated data of polydisperse rod-like and worm-like polymers generated according to the theory of Janmey for $Q = 16$, with statistical and systematic noise (0.05% with alternating ± signs) noise added.

		Rod-like single stranded (RLSS) polymers			
		Conversion degree p (% total rms noise added)			
Polynomial Fitting	Parameter	0.008 (0.94)	0.061 (0.64)	0.138 (0.42)	0.262 (0.28)
1st degree	M_w	1.00 ± 0.00	0.98 ± 0.01	ND	ND
	$<R_g^2>_z$	0.99 ± 0.02	0.74 ± 0.09		
	(χ^2)	(1.12 ± 0.32)	(9.96 ± 3.55)		
3rd degree	M_w	1.00 ± 0.00	1.00 ± 0.00	0.97 ± 0.00	0.83 ± 0.00
	$<R_g^2>_z$	0.89 ± 0.16	0.95 ± 0.04	0.78 ± 0.00	0.56 ± 0.00
	(χ^2)	(1.01 ± 0.40)	(1.33 ± 0.37)	(6.10 ± 1.19)	(116 ± 5.89)
4th degree	M_w	1.00 ± 0.00	1.00 ± 0.00	0.98 ± 0.00	0.87 ± 0.00
	$<R_g^2>_z$	0.92 ± 0.47	1.02 ± 0.07	0.85 ± 0.01	0.65 ± 0.00
	(χ^2)	(1.03 ± 0.44)	(1.30 ± 0.25)	(2.11 ± 8.51)	(30.5 ± 2.99)
5th degree	M_w	1.00 ± 0.00	1.00 ± 0.00	0.99 ± 0.00	0.91 ± 0.00
	$<R_g^2>_z$	0.94 ± 0.93	1.08 ± 0.18	0.91 ± 0.02	0.71 ± 0.00
	(χ^2)	(1.01 ± 0.45)	(1.29 ± 0.24)	(1.33 ± 0.41)	(9.32 ± 1.88)

(Table 2 continued)

		Worm-like single stranded (WLSS) polymers (l_p = 200 nm)			
		Conversion degree p (% total rms noise added)			
Polynomial Fitting	Parameter	0.008 (0.98)	0.061 (0.54)	0.138 (0.51)	0.262 (0.27)
1st degree	M_w	1.00 ± 0.00	0.99 ± 0.00		
	$<R_g^2>_z$	1.00 ± 0.01	0.79 ± 0.00	ND	ND
	(χ^2)	(1.11 ± 3.19)	(6.62 ± 0.86)		
3rd degree	M_w	1.00 ± 0.00	1.00 ± 0.00	0.99 ± 0.00	0.96 ± 0.00
	$<R_g^2>_z$	0.95 ± 0.25	0.98 ± 0.05	0.94 ± 0.01	0.90 ± 0.00
	(χ^2)	(1.17 ± 0.39)	(1.07 ± 0.43)	(1.65 ± 0.51)	(26.3 ± 2.76)
4th degree	M_w			1.00 ± 0.00	0.99 ± 0.00
	$<R_g^2>_z$	ND	ND	0.97 ± 0.02	0.97 ± 0.00
	(χ^2)			(1.17 ± 0.28)	(2.98 ± 0.58)
5th degree	M_w				1.00 ± 0.00
	$<R_g^2>_z$	ND	ND	ND	0.99 ± 0.00
	(χ^2)				(1.62 ± 0.54)

A different situation is found when the broader Janmey Q = 16 distributions are examined. For the rigid rod polymers, even the recovery of M_w becomes problematic at the higher p examined, 0.262, with a 5th degree polynomial faring no better than –9%. The same polynomial recovers the $<R_g^2>_z$ with a –30% error, while it performs better at p = 0.138, although a –10% error is still present. As already pointed out in the examination of Fig. 4, we are operating in a region where the $q^2<R_g^2>_z$ product indicates that only the first 4-5 angles, for p = 0.138, or only the first angle, for p = 0.262, lay in the region where the Zimm approximation is truly valid. However, when the worm-like polymers with l_p = 200 nm were considered, the situation was much improved, and even a 3rd degree polynomial could satisfactorily recover $<R_g^2>_z$, e.g. within 10%, across the whole spectrum of p examined.

Obviously, higher degree polynomials performed better at $p = 0.262$, a 4th degree returning the $<R_g^2>_z$ value within 3%.

Due to the crucial role played by the lower scattering angles in shaping the polynomial fitting outcome, we have also carried out a test on how an increased level of systematic noise on the first detector could influence the recovery especially of $<R_g^2>_z$. The results are shown in Table 3, where a 10-fold higher level of systematic noise, with either + or - sign, was superimposed to the statistical noise on the first detector only. We have selected only one of our conditions, e.g. an ensemble of rod-like polymers characterized by a Janmey $Q = 16$ distribution for $p = 0.138$, which is at the limit of the polynomial fitting capability. The corresponding results for the "normal" amount of systematic noise on the first detector, taken from the third column of the first part of Table 2, are also shown again for direct comparison. As can be seen, the effect is quite low, and mostly felt by the 5th degree polynomial, as could be expected.

Table 3. Effect of relevant systematic noise on the ratios between recovered and expected parameters for polynomial fittings in the $Kc/R\theta$ versus q^2 plots. The data refer to polydisperse rod-like polymers ($p = 0.138$) generated according to the theory of Janmey for $Q = 16$, with a statistical noise level of 0.46% rms. In addition, systematic noise (0.05% with alternating ± signs) was added to all angles, except the first, for which +0.05, +0.5 and -0.5% values were alternatively chosen.

Systematic noise on 1st detector	Parameter	Polynomial fitting		
		3rd degree	4th degree	5th degree
+0.05	M_w	0.97 ± 0.00	0.98 ± 0.00	0.99 ± 0.00
	$<R_g^2>_z$	0.78 ± 0.00	0.85 ± 0.01	0.91 ± 0.02
	(χ^2)	(6.10 ± 1.19)	(2.11 ± 8.51)	(1.33 ± 0.41)
+0.5	M_w	0.97 ± 0.00	0.99 ± 0.00	1.00 ± 0.01
	$<R_g^2>_z$	0.78 ± 0.01	0.87 ± 0.02	0.94 ± 0.03
	(χ^2)	(7.98 ± 1.78)	(2.61 ± 0.95)	(1.44 ± 0.80)
-0.5	M_w	0.96 ± 0.00	0.98 ± 0.00	0.99 ± 0.00
	$<R_g^2>_z$	0.77 ± 0.01	0.84 ± 0.01	0.90 ± 0.02
	(χ^2)	(5.19 ± 1.05)	(1.92 ± 0.65)	(1.22 ± 0.54)

B – Casassa and Holtzer plots.

In Fig. 5 the same synthetic, noise-free $Kc/R(q)$ data of Fig. 4 are plotted against q (Casassa plots). As can be seen, the data derived from the Flory distributions have initially a large non-linear portion, which becomes smaller as p increases. However, one would be tempted to extrapolate a M_L value from the linear portions (indicated by the center-filled symbols and by the regression lines), but this procedure can lead to quite erroneous results.

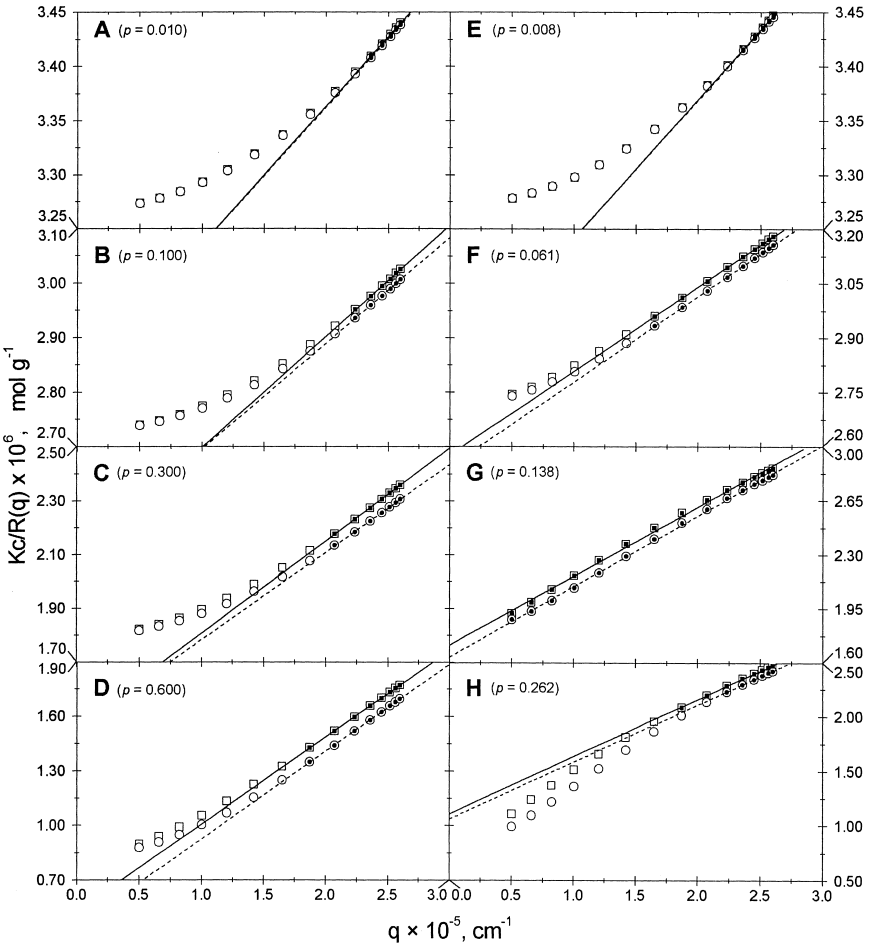

Fig. 5: Casassa plots of the same data presented in Fig. 4. Squares and continuos lines, rod-like polymers. Circles and dashed lines, worm-like polymers with $l_p = 200$ nm. The center-filled symbols denote the points included in the linear regressions. Panels A-D, Flory distributions, panels E-H Janmey distributions with $Q = 16$ (the conversion degree p is indicated in each panel).

In fact, by comparing panels A-D in Fig. 5 with the corresponding panels in the Holtzer plots reported in Fig. 6, one notices that only at the highest p examined, 0.6, the Holtzer plots are beginning to show a somewhat asymptotic behavior, although still 20-25% lower than the theoretical value of 6,000 g mol^{-1} nm^{-1}. This is understandable, considering that the large portion of shorter polymers still present at this p value (see Fig. 3), will contribute to the Casassa plot well outside of its asymptotic region. In order to better define this issue, in Table 4 we have collected the ratios between the values extrapolated from the linear fittings of Fig. 5 and the true M_L of the polymers.

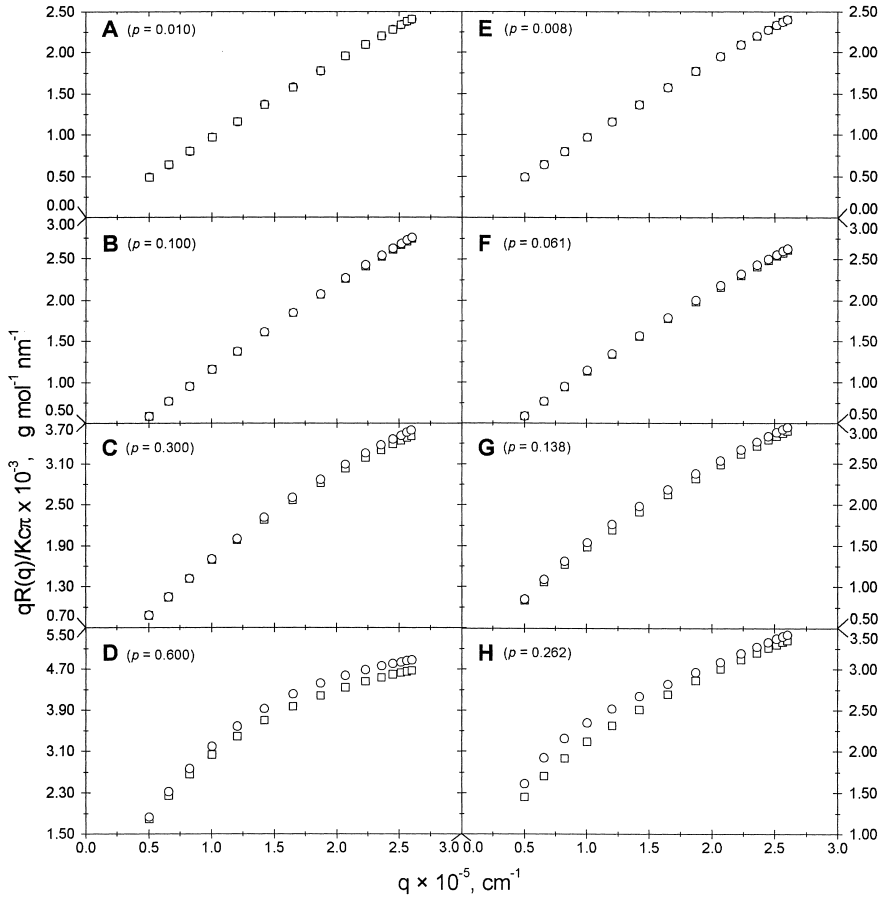

Fig. 6: Holtzer plots of the same data presented in Figs 4 and 5. Squares, rod-like polymers. Circles, worm-like polymers with l_p = 200 nm. Panels A-D, Flory distributions, panels E-H Janmey distributions with Q = 16 (the conversion degree p is indicated in each panel).

Table 4. Ratios between recovered and theoretical M_L obtained by the linear fittings of portions of the $Kc/R\theta$ versus q plots for the simulated data of polydisperse rod-like and worm-like polymers presented in Fig. 5.

	Conversion degree p, Flory distributions							
	0.010		0.100		0.300		0.600	
Polymers	M_L ratio	Detectors included	M_L ratio	Detectors included	M_L ratio	Detectors included	M_L ratio	Detectors included
RLSS	4.19	11 – 15	2.61	10 – 15	1.54	9 – 15	1.11	8 – 15
WLSS	4.32	10 – 15	2.74	10 – 15	1.63	9 – 15	1.13	8 – 15
	Conversion degree p, Janmey distributions with Q = 16							
	0.008		0.061		0.138		0.262	
Polymers	M_L ratio	Detectors included	M_L ratio	Detectors included	M_L ratio	Detectors included	M_L ratio	Detectors included
RLSS	4.15	11 – 15	2.29	7 – 15	1.16	1 – 15	1.01	8 – 15
WLSS	4.18	11 – 15	2.26	7 – 15	1.15	1 – 15	1.01	10 – 15

As can be seen in the first half of Table 4, the extrapolation of the linear portions of the Casassa plots for the Flory distributions initially leads to huge errors in M_L. Eventually, they decrease as the polymerization proceeds, but only for $p = 0.6$ they begin to be reliable, in conjunction with the appearance of a clear asymptotic trend in the corresponding Holtzer plot. A striking behavior was instead observed for the Janmey $Q = 16$ distributions for the Casassa plots reported on panels E-H of Fig. 5. While their linear portion increased more rapidly than the corresponding Flory distributions for a given M_w (compare panels B and F), a reversal of the curvature begins to take shape at relatively low p values (see panels C and G), and is fully evident at the highest p considered here. Conversely, only a mild hint of asymptotic behavior begins to take place in the last two panels (G and H) of the Holtzer plots in Fig. 6. Even more striking is the fact that the M_L is recovered within 16% already at $p = 0.138$, and nearly fully at $p = 0.262$, while the Holtzer plot would indicate differently. This behavior is clearly an effect of the peculiar size distribution resulting from the different rate of activation of the two sites in the monomer, which favors the formation of longer polymers while depleting the intermediate region (see Fig. 3).

Discussion

In this paper we have analyzed the applicability of the Zimm method to the study of the polymerization process of rod-like monomers which give rise to a polydisperse solution of linear rod-like or worm-like chains. For such a system the recovery of M_w and $\langle R_g^2 \rangle_z$ is not straightforward because the Zimm plot becomes curved very soon in the course of the polymerization, and an ordinary linear regression of the data is highly inadequate. In addition, also the methods devised independently by Casassa and Holtzer for determining the mass/length ratio were discussed and some intriguing features were pointed out.

The investigations were carried out by means of numerical simulations in which the conditions encountered in an experiment with simultaneous detection of the scattered light at all the scattering angles, were matched as much as possible. Although these conditions may appear very particular, the findings of our simulations are more general and applicable to many other systems of polydisperse semi-flexible chains.

To summarize the findings of our simulations in a manner which goes beyond the particular system that we have investigated, it is convenient to define a wavevector q^* as the one at which the condition $q^{*2}\langle R_g^2 \rangle_z = 1$ is attained. Thus, depending on the location of q^* with respect to the range $[q_1, q_2]$ of the measure, three different scenarios are possible. The first one is when $q_2 << q^*$, implying that all the data fulfill the conditions for the applicability of the Zimm method via an ordinary linear regression. This occurs usually at the beginning of the polymerization process (small p) where, consequently, the data are very noisy. The use of higher polynomial fittings in this case is not advisable, since it leads to results which are highly unstable (for instance, see the $p = 0.008$ columns in Table 2). In the second case, when q^* enters the range of the measure ($q_1 \leq q^* \leq q_2$), the use of higher polynomials increases the accuracy on the recovered parameters, with better improvements (with respect to the linear fitting) as q^* moves from q_2 to q_1. The use of higher degrees also leads to higher accuracy, but at the same time renders the results more unstable with respect to noise. Thus, a tradeoff between accuracy and stability has to be made and, as rule of the thumb, we suggest to use always the smallest polynomial degree which gives results comparable (within the desired accuracy) to the next higher polynomial. Another point which can be made by looking at Table 2, is that one should not use a higher degree polynomial without an appreciable reduction of the reduced χ^2. Lastly, when $q^* \leq q_1$, the applicability of the Zimm technique is severely jeopardized and to force its use is definitively not advisable. An example of its improper use has been given for the RLSS polymers reported in panel H of Fig. 4 (see also Table 2).

The analysis of the Casassa and Holtzer plots was done much less thoroughly than the one carried out for Zimm plots. Our main purpose was to point out that an estimate of the ratio M_L based on the analysis of Casassa alone is not advisable, and may lead to quite erroneous results. Thus, a cross check with the behavior of the corresponding Holtzer plot is of fundamental importance for discerning whether the recovered M_L is reliable or not. If the Holtzer plot is still far away from having attained its asymptotic behavior when the Casassa plot is already close to linearity, the extrapolated M_L is likely to be unreliable. Conversely, if both the Casassa and Holtzer plots are both reasonably close to their asymptotic behaviors, the recovered M_L is probably reliable. This is what it can be expected from the master curves of Fig. 2 and it is what happens for "well behaved" distributions such as the Flory distributions. But this is not always the case. Effects of polymer polydispersity might be responsible for some peculiar appearance of the Casassa plot. As shown for the Janmey $Q = 16$ distributions of Fig. 5 (panels E-G), the Casassa plots exhibit a transition between their usual upward concavity to a downward one, and this makes them appear much more "linear" than the corresponding plots for Flory distributions. Remarkably, and at variance with what stated above for the Flory distributions, the M_L is recovered accurately in spite of the fact that the Holtzer plots are still far away from convergence. Thus even combining together Casassa and Holtzer plots may not be sufficient for discerning their correct range of applicability.

We would like to conclude by pointing out that the results here illustrated do not pretend to be an exhaustive investigation of the polynomial fitting technique. The main purpose of this work was to put in some evidence that a polynomial fitting of curved Zimm plots, when properly applied, may significantly improve and extend the applicability of the Zimm method. Many issues associated with this technique, such as, for example, the effect of noise, the optimization of how many points laying outside the Zimm region have to be included in the fitting, and a real criterion for choosing the polynomial degree, are still open and require a deeper understanding. To this end, more numerical simulations are currently in progress.

References

1. P. J. Flory, *Principles of Polymer Chemistry*, Cornell University Press, Ithaca, NY 1953
2. P. A. Janmey, *Biopolymers* **21**, 2253 (1982)
3. S. Bernocco, F. Ferri, A. Profumo, C. Cuniberti, M. Rocco, *Biophys. J.* **79**, 561 (2000)
4. R. F. Doolittle, *Annu. Rev. Biochem.* **53**, 195 (1984)
5. M. W. Mosesson, R. F. Doolittle (Eds.), *Molecular Biology of Fibrinogen and Fibrin,* Ann. New York Acad. Sci. Vol. 406, 1983
6. P. Wiltzius, G. Dietler, W. Känzig, V. Hoffmann, A. Häberli, P. W. Straub. *Biophys. J.* **38**, 123 (1982)

7. C. S. Johnson, D. A. Gabriel, in: *Spectroscopy in Biochemistry*, J. E. Bell (Ed.), CRC Press, Boca Raton FL 1981, c.5/178ff
8. B. H. Zimm, *J. Chem. Phys.* **16**, 1093 (1948)
9. E. F. Casassa, *J. Chem. Phys.* **23**, 596 (1955)
10. R. Koyama, *J. Phys. Soc. Jpn.* **34**, 1029 (1973)
11. M. Müller, W. Burchard, *Biochim. Biophys. Acta* **537**, 208 (1978)
12. H. Benoit, P. Doty, *J. Chem. Phys.* **57**, 958 (1953)